Supramolecular clustering of the cardiac sodium channel Nav1.5 in HEK293F cells, with and without the auxiliary β3-subunit.

Samantha C. Salvage[1*], Johanna S Rees[1], Alexandra McStea[2], Michael Hirsch[2], Lin Wang[2], Chris Tynan[2], Matthew W. Reed[3], Jennifer R. Irons[1], Richard Butler[4], Andrew J. Thompson[5], Marisa Martin-Fernandez[2], Christopher LH. Huang[1, 6*], Antony P. Jackson[1*].

[1]Deparment of Biochemistry, University of Cambridge, CB2 1QW, United Kingdom.

[2]Central Laser Facility, Research Complex at Harwell, Science and Technology Facilities Council, Rutherford Appleton Laboratory, Harwell, Didcot, Oxford, OX11 0QX, UK

[3]Department of Nuclear Physics, Research School of Physics and Engineering, Australian National University, ACT 2601.

[4]Wellcome Trust/Cancer Research UK Gurdon Institute, University of Cambridge, CB2 1QN, United Kingdom.

[5]Department of Pharmacology, University of Cambridge, CB2 1PD, United Kingdom.

[6]Department of Physiology, Development and Neuroscience, University of Cambridge, CB2 3EG United Kingdom.

*Corresponding authors.

Short title: Oligomerisation of Nav1.5-β3 complex in vivo.

Abbreviations:

AFM	Atomic Force Microscopy
BrS	Brugada syndrome
β3	Voltage gated sodium channel beta 3 subunit
Co-IP	Co-immunoprecipitation
C_m	Membrane capacitance
DDM	n-Dodecyl β-D-maltoside
DTT	Dithiothreitol
E_{Na}	Na^+ reversal potential
EGFP	Enhanced Green Fluorescent Protein
ER	Endoplasmic Reticulum
ERAD	Endoplasmic Reticulum associated degradation
FBS	Fetal Bovine Serum
FRET	Fluorescence resonance emission transfer
G	Conductance
G/G_{max}	Normalised conductance
HBSS	Hanks' balanced salt solution
HEK	Human Embryonic Kidney cells
Ig	Immunoglobulin
I	Current
LQTS	Long QT syndrome
Nav1.5	Cardiac voltage gated sodium channel
PBS	Phosphate buffered saline
PEI	Polyethylenimine
PFA	Paraformaldehyde
PLA	Proximity Ligation Assay
PSF	Point Spread Function
SEM	Standard Error of the Mean
STORM	Stochastic Optical Reconstruction Microscopy
TCEP	Tris(2-carboxyethyl) phosphine
TBST	Tris buffered saline with Tween20

Abstract:

Voltage-gated sodium channels comprise an ion-selective α-subunit and one or more associated β-subunits. The β3-subunit (encoded by the SCN3B gene) is an important physiological regulator of the heart-specific sodium channel, Nav1.5. We have previously shown that when expressed alone in HEK293F cells, the full-length β3-subunit forms trimers in the plasma membrane. We extend this result with biochemical assays and use the proximity ligation assay (PLA) to identify oligomeric β3-subunits, not just at the plasma membrane, but throughout the secretory pathway. We then investigate the corresponding clustering properties of the α-subunit and the effects upon these of the β3-subunits. The oligomeric status of the Nav1.5 α-subunit *in vivo*, with or without the β3-subunit has not been previously investigated.

Using super-resolution fluorescence imaging, we show that under conditions typically used in electrophysiological studies, the Nav1.5 α-subunit assembles on the plasma membrane of HEK293F cells into spatially localised clusters rather than individual and randomly dispersed molecules. Quantitative analysis indicates that the β3-subunit is not required for this clustering but β3 does significantly change the distribution of cluster sizes and nearest neighbor distances between Nav1.5 α-subunits. However, when assayed by PLA, the β3-subunit increases the number of PLA-positive signals generated by anti-(Nav1.5 α-subunit) antibodies, mainly at the plasma membrane. Since PLA can be sensitive to the orientation of proteins within a cluster, we suggest that the β3-subunit introduces a significant change in the relative alignment of individual Nav1.5 α-subunits, but the clustering itself depends on other factors. We also show that these structural and higher-order changes induced by the β3-subunit do not alter the degree of electrophysiological gating co-operativity between Nav1.5 α-subunits. Our data provides new insights into the role of the β3-subunit and the supramolecular organisation of sodium channels, in an important model cell system that is widely used to study Nav channel behaviour.

Introduction:

The cardiac voltage-gated sodium channel (Nav1.5) is crucial for the generation and conduction of the cardiac action potential. Nav1.5 is a transmembrane protein that comprises a large pore-forming, sodium-selective α-subunit that contains four homologous domains (DI - DIV). Each domain consists of six membrane spanning alpha helices (S1 - S6). In each domain, helices S1-S4 form the voltage-sensor regions. The S4 helix contains positively charged residues that enable it to move in response to changes in the membrane potential. This movement drives further conformational changes, leading to transient channel opening, quickly followed by channel inactivation (1). Movement of the S4 segments of DI - DIII have been associated with the activation step, while S4 of DIV is associated with inactivation, consistent with the m^3h model of Hodgkin and Huxley (2).

There are four Nav channel β-subunit genes (SCN1B-4B) encoding proteins β1 - β4(3). All the β-subunits - except a an alternatively spliced β1b isoform - contain an extracellular immunoglobulin (Ig) domain connected *via* a small flexible neck to a single transmembrane spanning alpha-helical region and a short intracellular C-terminal tail. The β-subunits influence Nav channel activity through effects on the voltage-sensitivity of activation and inactivation, the kinetics of channel activation and inactivation, as well as indirect effects such as alterations in the trafficking of channels from the endoplasmic reticulum (ER) to the plasma membrane. However, individual β-subunit isoforms modify these parameters to different extents, often in a cell-specific manner (4–6).

Expression of the β3-subunit is most abundant in the ventricles of the heart (4) and the importance of β3-subunit regulation of Nav1.5 is particularly apparent in ventricular arrhythmic syndromes, including Brugada syndrome (BrS) and Long QT syndrome (LQTS). This has been experimentally modelled in the β3-knockout (*Scn3b*$^{-/-}$) murine cardiac model which shows a BrS-like phenotype that includes a reduction of peak sodium current density (I_{Na}), abnormal ventricular electrophysiological characteristics, alterations in sino-atrial node (SAN) function and abnormal atrial conduction (7, 8). Similarly, a number of SCN3B gene mutations have been identified in cases of BrS in which the Nav1.5 protein is apparently normal (9).

The atomic-resolution structure of the β3-subunit Ig domain suggests that it can form trimers when expressed in HEK293F cells. Moreover, images of immuno-purified channels obtained by atomic force microscopy (AFM), indicate that the β3-subunit can bind at up to four sites, symmetrically arranged around the Nav1.5 α-subunit (10). This implies a more complex and perhaps variable stoichiometry between these two channel components than has traditionally been assumed. However, it is not yet clear if this complexity can contribute to higher-order associations between Nav1.5 channels.

Here we use cell-biological, biochemical and super-resolution imaging approaches to further investigate the oligomeric status of the β3-subunit and its effect on the *in vivo* organisation of Nav1.5 α-subunits. We find that in the HEK293F cell-line model, commonly used in electrophysiological assays, the Nav1.5 α-subunit forms oligomeric complexes on the plasma membrane even in the absence of β3. However, the β3-subunit does modulate the organisation of individual Nav1.5 α-subunits within the clusters, whilst not altering the degree of gating co-operativity between individual α-subunits. Our work identifies an unexpected property of Nav1.5 channels in a cell system routinely used for electrophysiological studies and raises new questions about the control of Nav channel clustering.

Materials and Methods:

Cell culture, DNA constructs and transfections:

Human embryonic kidney (HEK293F) cells and HEK293F cells stably expressing Nav1.5 (HEK293F-Nav1.5) were maintained in DMEM (DMEM/F-12 Glutamax, Invitrogen, UK) with 10% FBS (Sigma-Aldrich, UK) at 37°C and 5% CO_2. The plasmids pcDNA3-Nav1.5-hemagglutinin (HA), pcDNA3 Nav1.5-green fluorescent protein (GFP), pEnhanced Green Fluorescent Protein (EGFP), pEGFP-β3 and pFBM β3-myc have all been previously described (11–13). Transient transfections were performed using polyethylenimine (PEI, 1μg/μl) at a PEI / DNA ratio of 3:1.

For whole cell patch clamp electrophysiology, HEK293F-Nav1.5 cells were plated on 18 mm coverslips in 6-well plates and transiently transfected with either 1 μg of the empty vector pEGFP-N1 or pEGFP-β3.

Transient transfections for biochemical experiments were carried out on either HEK293F or HEK293F-Nav1.5 in 100 mm dishes at 70 - 80 % confluency. For co-immunoprecipitation studies, HEK293F cells were transfected with either 4 μg of β3-EGFP or β3-myc alone, or co-transfected with 4 μg each. Proximity ligation assay and immunohistochemistry experiments were performed on HEK293F cells transfected with 3 μg each of Nav1.5 H.A and Nav1.5 EGFP ± 3 μg of β3-myc.

For STORM experiments, HEK293F cells were plated in 35 mm glass (no 1.) bottom dishes and transfected at around 70% confluency with Nav1.5 HA (0.5 μg) and either β3-EGFP (0.5 μg) or EGFP (0.5 μg)

Co-immunoprecipitation:

Forty-eight hours post transfection, cells were washed 3× in cold phosphate buffered saline (PBS, ThermoFisher, UK) then lysed in 1 ml lysis buffer (Tris 50 mM, NaCl 150 mM, 1 % Triton x-100 (v / v)) supplemented with protease inhibitor cocktail (Roche, Sigma-Aldrich, UK). Lysates were vortexed and mixed with end-over-end rotation at 4°C for 30 mins, centrifuged at 10,000 *g* for 10 mins at 4°C and the pellet (cell debris) fraction discarded. Lysates were incubated with either mouse anti-myc tag, mouse anti-GFP tag or mouse anti-HA with end over end rotation at 4°C overnight, followed by the addition of Protein G agarose for 4 hours. The samples were spun at 2,000 *g* at 4°C for 5 min. Pellet (bound) fractions were washed 4× in 1 ml lysis buffer and both these and the supernatants (unbound) were incubated in 4× NuPage loading buffer supplemented with dithiothreitol (DTT) at 85 °C for 10 mins. The bound and unbound fractions were separated on SDS-PAGE, transferred to nitrocellulose membranes (iBlot transfer system, ThermoFisher Scientific) and Western blots carried out with rabbit polyclonal antibodies; anti-EGFP (GeneTex, Insight Biotech, UK) and anti-myc (Santa Cruz, Insight Biotech, UK) were used to detect β3-EGFP and β3-myc respectively.

Cross-linking experiments:

HEK293F cells transfected with 4 μg of either β3-EGFP or β3-myc were washed 3× in Hanks' balanced salt solution (HBSS, ThermoFisher, UK) and lysed in 1 ml of HBSS lysis buffer (1% Triton x-100, 0.2% sodium dodecyl sulphate (SDS), 0.5% sodium deoxycholate) with protease inhibitors (Complete Protease inhibitor cocktail, Roche). The lysates were split into two equal fractions; a control had nothing added, and to the other, 5 mM bis(sulfosuccinimidyl) suberate (BS3; an amine-to-amine crosslinker), was added and incubated at 4 °C for 1 hr with end over end rotation. The reaction was quenched with 74 mM glycine and clarified at 10,000 *g* for 10 mins at 4°C. Samples were then subject to SDS-PAGE and Western blot as previously described.

Super-resolution STORM imaging:

HEK293F-Nav1.5 cells co-transfected with Nav1.5-HA and β3-EGFP or EGFP were washed 3× in cold PBS and then fixed with 4 % paraformaldehyde (PFA) for 10 - 15 mins. PFA was rinsed off with PBS, the cells were permeabilised in 0.1% (v/v) Triton x-100 in PBS for 10 min followed by blocking with 1 % BSA for 1 hr at room temperature. Primary antibody (mouse monoclonal anti-HA, sc-7392, Santa Cruz) was incubated at 4 °C overnight. Then 4x 10-15 min washes in PBST (PBS supplemented with 0.1% Tween20). Secondary antibody (goat anti-mouse IgG Alexa647, Invitrogen, ThermoFisher, UK) was incubated for 1 hr at room temperature followed by 4x 10-15 min washes in PBST and stored in PBS at 4°C until ready for STORM.

The super-resolution STORM images were taken on a Zeiss Elyra PS.1 system. The fluorophore Alexa Fluor 647 was photo-switched using 642 nm excitation laser, with 100 mM dithiothreitol in PBS as the switching buffer. The power density of the 642 nm illumination on the sample plane were about 5.5 kW/cm^2. A 100× NA 1.46 oil immersion objective lens (Zeiss alpha Plan-Apochromat) witha two-color notch filter (561/642 nm) was used as dichroic mirror in the imaging. The final fluorescent images were projected on an Andor iXon 897 EMCCD camera.

Super-resolution STORM images were reconstructed and rendered in ZEISS ZEN software. The PALM function in ZEN allows filters to be set for peak finding and choosing a fit model for the localization calculation. In STORM image processing, 9 pixels of peak mask size were applied according to pixel resolution and PSF size in the data sets. The peak intensity to noise filter was set to 6 as this was efficient to identify peaks from background. The fit model was a two-dimensional Gaussian fit, and only single emitters from fluorophores were taken into account, whereas all multiple emitters were discarded. Following the localization, the displacements of molecules from drifts in the reconstructed images were corrected for using feature detection and cross correlation.

The clustering analysis was conducted as described in (14), data analysis section A "Analysis using Bayesian Cluster Algorithm". We selected 12 regions of interest (ROIs), with a total of 199589 observations for cells expressing Nav1.5 alone and 16 ROIs with a total of 272678 observations for cells co-expressing Nav1.5 and β3-subunit. The algorithm reports for each cluster the cluster radius and the number of molecules in the cluster.

The summaries include the data of all clusters found in the ROIs. The nearest neighbor analysis employs a standard k-d tree. The nearest neighbor for all observations in the ROIs were calculated as described (14). The nearest neighbor may have been outside the ROI where the observation was located near the edge of the ROI. Comparisons of radii and nearest-neighbor distributions for clusters with Nav1.5 alone and clusters with Nav1.5 and β3-subunit were tested for whether these distributions were identical using the two-sample Kolmogorov–Smirnov (KS) test, which compares the samples from the two conditions without the need for a reference distribution (15).

Proximity ligation assay (PLA):

Twenty-four hours post transfection cells were transferred to poly-l-lysine coated glass coverslips and left for a further twenty-four hours. Cells were then washed 3× in cold phosphate buffered saline (PBS, ThermoFisher, UK) and fixed with 4 % paraformaldehyde (PFA) for 10 - 15 mins. PFA was rinsed off with PBS, the cells were permeabilised in 0.1% (v/v) Triton x-100 in PBS for 10 min followed by blocking with 1 % BSA for 1 hr at room temperature. Primary antibodies were incubated at 4 °C overnight and the procedure carried out according to the manufacturer's instructions (Duolink, Sigma). Briefly, cells were washed, then incubated with PLA probes (specific to the species of the primary antibodies) at 37 °C in a humidity chamber. This was followed by a 30 min ligation step at 37 °C, and an amplification step of 100 min at 37°C with intervening washes. Coverslips were mounted to glass slides with the supplied DAPI mounting media, sealed with clear nail polish and viewed on an Olympus FV1000 confocal microscope. DAPI, GFP and AlexaFluor594 were observed. The 488 nm and 559 nm laser lines were used in a sequential manner to prevent bleed through of signals. A custom Python script for Fiji(16) was used to enable automated analysis of the PLA data. The script maps the volumes of DAPI and Nav1.5-GFP signals using a 3D Gaussian blur (sigma= DAPI; 0.5 and EGFP; 0.25) to reduce the effects of noise and the Triangle thresholding algorithm to generate binary masks. PLA signal dots, indicative of protein proximity, were mapped by subtracting the 3×3×1 3D maximum filtered signal from the original, then detecting local maxima with a noise tolerance of 15. These detected points were used to measure the values of the exact signed Euclidean distance transform of the DAPI mask as well as the signal intensity values in the Nav1.5-GFP and PLA channels. These measurements allowed us to calculate the PLA dot count per Nav1.5-GFP positive cell. In addition PLA signal intensity was determined using the online freely available software 'BlobFinder'(17).

Whole cell patch clamp:

Na^+ currents (I_{Na}) were recorded from HEK293F cells stably expressing Nav1.5 and transiently transfected with either a vector containing only EGFP (Nav1.5 + EGFP), or β3-EGFP (Nav1.5 + β3-EGFP). Successfully transfected cells were identified by EGFP fluorescence on an Olympus IX71 inverted microscope. Experiments were carried out at room temperature (22 - 23°C) in the whole cell configuration with an Axopatch 200B amplifier (Axon instruments, California, US), a Digidata 1322A digitizer (Axon instruments, California, US) and the Strathclyde Electrophysiology Software Package (WinWCP, Department of

Physiology and Pharmacology, University of Strathclyde). The extracellular bath solution contained (in mM): NaCl 60, KCl 2, $CaCl_2$ 1.5, glucose 10, $MgCl_2$ 1, $CsCl_2$ 90, HEPES 10, pH 7.39 ± 0.02 with NaOH. 1.5 – 2.5 MΩ patch pipettes were produced from borosilicate glass capillaries (Harvard Apparatus Ltd, UK) using a horizontal puller (P-87 Sutter Instruments, CA, USA) and filled with intracellular saline, comprised of (in mM): NaCl 35, CsF 105, EGTA 10, HEPES 10, pH 7.39 ± 0.02 with CsOH. Signals were low pass Bessel filtered at a frequency of 5 kHz and sampled at 125 kHz. Series resistance compensation was performed to 75 - 80% and leak currents were subtracted using a P / 4 protocol. The liquid junction potential (2 mV) was not corrected for. Data from cells with a current amplitude larger than 8 nA, or with a clear loss of voltage control as demonstrated by poor *I*/V relationships were removed.

Voltage protocols:

Voltage protocols used a holding voltage of -120 mV. The activation protocol consisted of a 50 ms depolarising test pulse ranging from – 90 mV to +35 mV, in 5 mV increments. The resulting current traces were normalised against the whole cell capacitance (C_m) and the *I*/V relationship plotted from peak current at each test voltage. Values of Na^+ conductance (G_{Na}), for families of traces at each test voltage, were determined from the equation;

$$\boldsymbol{G_{Na} = I_{Na}/(V - E_{Na})} \quad (1)$$

where I_{Na} is the Na^+ current and E_{Na} is the Na^+ reversal potential. Peak G_{Na} was plotted as a function of voltage to produce activation curves.

Steady-state inactivation was assessed with 100 ms conditioning pre-pulses ranging from -140 mV to -50 mV in 5 mV increments followed immediately by a 50 ms depolarising test pulse to -40 mV. I_{Na} was normalised to the maximum elicited current and plotted against the conditioning voltage to yield inactivation curves. Both curves were fitted to the following Boltzmann function;

$$\boldsymbol{G/G_{max} = 1/(1 + exp((V - V_{½})/k))} \quad (2)$$

where G/G_{max} is the normalised conductance or current, $V_{½}$ is the voltage of half-maximal activation or inactivation, *k* is the slope factor and *V* is the test voltage or conditioning voltage.

Recovery from inactivation was examined using a double pulse protocol that delivered two identical depolarizing pulses to -40 mV (P1 and P2) of 50 ms duration. The time interval between P1 and P2 was incremented by 3 ms with each successive sweep up to a maximum interval of 72 ms. Peak currents from P2 were normalized to those obtained in response to the conditioning P1 step and plotted against the time intervals. These plots were fitted with a mono-exponential function as follows;

$$\boldsymbol{I_{P2}/I_{P1} = 1 - \exp(-t/\tau)} \quad (3)$$

where *t* is the time and τ the time constant of recovery from inactivation.

Analysis of Na^+ current kinetics.

Families of G_{Na}, in response to each voltage step or conditioning voltage were then fitted to the standard solution for the time-course of G_{Na} employing the established Hodgkin-Huxley m^3h formulation:

$$\boldsymbol{G_{Na} = \overline{G_{Na}}\left(m_{\infty} - (m_{\infty} - m_0)e^{-t/\tau_m}\right)^3\left(h_{\infty} - (h_{\infty} - h_0)e^{-t/\tau_h}\right) + offset} \qquad (4)$$

where the maximum steady state conductance term $\overline{G_{Na}}$ was derived from the voltage step that yielded the maximum peak I_{Na} in the patch studied. The terms m and h represent the Hodgkin-Huxley activation and inactivation variables. These have time constants τ_m and τ_h respectively, describing the decay in their respective variables in response to either the activating or inactivating voltage step imposed at time = 0, to the steady state, t = ∞, following the voltage step. The offset term in the equation allowed for the finite membrane conductance. The gating variables m_0 and m_∞, were obtained from the cube root of the previously determined G/G_{max} values from the activation function (equation 2) whose values of $V_{½}$ and k were derived at each voltage preceding and immediately following the voltage step. Similarly, h_0 and h_∞ were obtained directly from the G/G_{max} values in the steady-state inactivation function for the voltage preceding and immediately following the voltage step. These fits allowed for the derivation of the activation (τ_m) and inactivation (τ_m) decay constants.

The time course of current decay was determined using the following double exponential fit;

$$\boldsymbol{y = -A_1\exp(-t/\tau_1) - A_2\exp(-t/\tau_2)} \qquad (5)$$

where A_1 and A_2 are the magnitudes of the fast and slow currents, respectively, and τ_1 and τ_2 are the corresponding time constants. Peak currents were measured using WinWCP v 5.0.9 and analysed in Prism v.7. For m^3h analysis and time constants of inactivation, raw data was exported and analysed through a custom Python script.

Results:

Oligomerisation of the β3-subunit when expressed in HEK293F cells

We have previously shown that the β3-subunit, expressed in HEK293F cells can form trimers on the plasma membrane surface (10). However, the stability and extent of this interaction is not clear. Neither is it clear whether the β3-subunit oligomerisation occurs only on the plasma membrane. To investigate these questions, we performed co-immunoprecipitation on lysates from HEK293F cells co-transfected with two differently tagged β3 constructs; β3-EGFP and β3-myc. As a control, single transfection of the β3-myc construct was performed. The smaller size of myc relative to EGFP results in a mobility shift which allows for the discrimination of the two β3-subunits on a Western blot; β3-myc migrates further than β3-EGFP (30–35 kDa shift). The β3-EGFP subunit was immunoprecipitated with a mouse anti-GFP antibody/protein G agarose mixture and found in the bound fraction in all cell lysates in which it was transfected (Fig. 1A). This mixture was saturated and thus β3-EGFP was also found in the unbound supernatant fraction. Crucially, co-immunoprecipitation of β3-myc only occurred in the presence of β3-EGFP; when β3-myc was transfected alone it was only found in the unbound, supernatant fraction (Fig. 1A).

The cell-lysates from cells separately transfected with β3-myc and β3-EGFP were cross-linked with BS3 and examined by western blotting (Fig. 1B). Cross-linking of β3-myc produced large distinct bands at approximately 35, 70 and 105 kDa, while cross-linking of β3-EGFP resulted in bands at approximately 60, 120 and 180 kDa; in both cases indicative of monomers, dimers and trimers respectively. There was additional, less intense, smearing travelling upwards from the monomeric bands in both samples, and to a lesser degree in both the dimeric and trimeric bands, which are likely post-translational modifications, such as glycosylation. The different migratory patterns between the two tagged β3-subunits can be attributed to the differing sizes of the myc (1-2 kDa) and EGFP (30-32 kDa) tags. Thus, the oligomeric interaction between β3-subunits is sufficiently stable to survive cell-lysis and the prolonged washing steps inherent in immunoprecipitation experiments. Furthermore, under these conditions, the β3-subunits is capable of forming dimers and trimers, rather than aggregates of indeterminate stoichiometry.

To assess the cellular compartments where β3-subunit oligomerisation occurs *in situ*, we used the proximity ligation assay (PLA). This method employs two antibodies from different species targeting different epitope tags on co-expressed β3-subunits. Secondary antibodies raised against each primary antibody and conjugated to a matched pair of short single-stranded oligonucleotides are added. If the two respective targets are within about 20 nm, the oligonucleotide probes will hybridize with a "bridging oligonucleotide" to form a continuous circular DNA structure, which can be amplified by DNA polymerase and detected by a fluorescently labelled oligonucleotide (18). Co-transfection of β3-EGFP and β3-myc, each tagged with one of the PLA probes post-fixation, produced characteristic punctate staining in the red (597 nm) channel, indicating that co-transfected β3-EGFP and β3-myc resided within 20 nm of each other (Fig. 1C). Labelling was heavy and not just restricted to the plasma membrane, but also occurred internally, especially in large perinuclear regions consistent with

endoplasmic reticulum and other compartments within the secretory pathway. No discernible PLA signal was observed when either β3-EGFP or of β3-myc was expressed alone, indicating that the PLA probes showed no non-specific binding (Fig. 1C). Thus, the β3-subunits have a natural tendency to oligomerise when expressed in HEK293F cells, and this occurs at an early part of the secretory pathway.

Formation of Nav1.5 complexes in situ.

To examine the oligomeric state of Nav1.5, we transiently expressed HA-epitope tagged Nav1.5 α-subunits in HEK293F cells, with or without EGFP-tagged β3-subunit and examined their distribution on the plasma membrane using super-resolution STORM imaging. Transfected cells were fixed and permeabilised and labelled with a monoclonal antibody against HA epitope, followed by Alexa Fluor 647-labelled second antibody as described in Materials and Methods. Typical labelling at the plasma membrane is shown in Fig. 2A. Surprisingly, Nav 1.5 α-subunits alone were not randomly dispersed on the plasma membrane but about 40% of the α-subunits assembled into larger multi-molecular clusters. The β3-subunit did not affect the proportion of oligomerised Nav1.5 α-subunits, nor did it affect the density of clusters on the plasma membrane (Fig. 2B, C). However, the β3-subunit did increase the proportion of larger-radii clusters (Fig. 2D). This difference was highly statistically significant (two-sample Kolmogorov-Smirnov test, $P = 4 \times 10^{-9}$). For the case of Nav 1.5 α-subunits expressed alone, the distribution of nearest-neighbor distances between α-subunits within clusters followed a positively skewed distribution, with a modal value ~ 6 nm. This pattern was still present in the nearest-neighbor distribution measured in the presence of the β3-subunit. However, now an additional peak with a modal value ~12 nm was also prominent (Fig. 2E). This difference was again highly significant (two-sample Kolmogorov-Smirnov test, $P \sim 0$).

For comparison, we also performed a PLA experiment to monitor α-subunit clustering. Since the efficiency of PLA can be very sensitive, both to the relative positions and relative accessibility of the two separate epitopes on separate proteins (18), the method may provide additional and complementary information on protein organisation within clusters. We used two differently tagged Nav1.5 α-subunits; Nav1.5-HA and Nav1.5-GFP, co-transfected with or without β3-myc (Fig. 3A). Although β3 was not required to generate PLA signals, it did increase the number of PLA dots detected (Fig. 3A, B). Interestingly, this PLA signal occurred predominantly at the plasma membrane, as observed in z-stack images (Fig. 3C). Immunostaining of Nav1.5-HA was also carried out to confirm that co-transfection of the β3-myc did not alter the expression of Nav1.5-HA and Nav1.5-GFP. Here, the level of HA- and GFP- tagged α-subunits were similar in cells with or without β3 (Supplementary Fig. S1). Taken together, this indicates that the β3-subunit is not required for Nav1.5 α-subunit clustering *per se* but does significantly influence the geometry and/or the relative orientation of channels within clusters.

Steady-state activation of the Na^+ channel is unaffected by its co-expression with the β3-subunit.

Typical examples of whole cell Na^+ currents (I_{Na}) from stably expressing Nav1.5-HEK293F cells transiently transfected with an empty EGFP vector (Nav1.5 + EGFP) or EGFP-tagged β3-subunit (Nav1.5 + β3-EGFP) in response to an incremental step depolarisation are illustrated in **(**Fig. 4A). The co-expression of the β3-subunit with Nav1.5 did not alter the amplitude of peak current ($I_{Na(max)}$; Nav1.5 + EGFP, 263.64 ± 27.70 pA / pF, Nav1.5 + β3-EGFP, 268.00 ± 21.89 pA / pF, $P > 0.05$). The current-voltage relationships yielded E_{Na} values in the absence and presence of the β3-subunit of 19.45 ± 0.98 mV and 19.58 ± 0.68 mV respectively (Fig. 4B). Both of these values are consistent with the value predicted from the Nernst potential (17.46 mV) corresponding to the known extracellular (~70 mM) and intracellular (35 mM) Na^+ concentrations. Activation curves were normalized to their maximum peak values (giving G/G_{max}) and divided by the driving force ($V-E_{Na}$) and yielded similar voltage-dependences ($V_{½}$; Nav1.5 + EGFP = -42.62 ± 1.81 mV, Nav1.5 + β3-EGFP = -42.61 ± 1.67 mV, means ± SEMs; $P > 0.05$), and slope factor (k; Nav1.5 + EGFP = 7.28 ± 0.61 mV, Nav1.5 + β3-EGFP = 9.42 ± 0.94 mV, $P > 0.05$, (Fig. 4B-C). Similarly, the maximal channel conductances (G_{max}) were similar ($P > 0.05$, Fig. 4C) for Nav1.5 alone (6.47 ± 0.21 mS / cm^2) and β3-EGFP (6.69 ± 0.32 mS / cm^2).

Co-expression of the β3-subunit induces a depolarising shift in the steady state voltage dependence of Na^+ channel inactivation.

Typical inactivation traces from Nav1.5 + EGFP and Nav1.5 + β3-EGFP are shown in (Fig. 5A). Co-expression of the β3-subunit resulted in a 5.5 mV depolarising shift of steady-state inactivation ($V_{½;}$ Nav1.5 + EGFP = -96.14 ± 0.72 mV; Nav1.5 + β3-EGFP = -90.64 ± 1.02; $P < 0.001$, (Fig. 5B). This depolarising shift was observed in the absence of any significant variation in k (Nav1.5 + EGFP = -7.17 ± 0.20; Nav1.5 + β3-EGFP = -6.47 ± 0.32 mV).

Co-expression of the β3-subunit does not alter the kinetics of Na^+ channel activation and inactivation.

The time constants for activation (m) and inactivation (h) were determined using the standard Hodgkin Huxley m^3h model (Eq. 4; Fig. 6). The time constants (τ_m) for m were indistinguishable between Nav1.5 + EGFP and Nav1.5 + β3-EGFP **(**Fig. 6A). Time constants for the inactivation parameter (τ_h) appeared to show subtle shifts in the presence of the β3-subunit (Fig. 6B), but when the voltage-dependences were corrected for the 5.5 mV shift previously observed in the steady-state inactivation curves, these time constants were comparable (Fig. 6C). However, some reports have described the inactivation process as a sum of two components; a rapid and slow decay (6, 12). Thus, we further assessed the decay of the Na^+ current with a double exponential function to find evidence for separate fast (τ_1) and slow (τ_2) time constants (Fig. 7A), and then similarly corrected for the relative shifts of steady-state inactivation (Fig. 7B). A double exponential fitted the inactivation process better than a single exponential with a fast component that demonstrated a voltage-dependence and a slow component that was relatively voltage-independent. Nevertheless, neither voltage-dependences of such rate constants were altered by the β3-subunit.

The β3-subunit accelerates the recovery of the Na^+ channel from inactivation.

Typical I_{Na} traces from Nav1.5 + EGFP and Nav1.5 + β3-EGFP in response to a double pulse protocol are shown in Fig. 8A. Peak currents of P2 normalised to peak currents of P1 were plotted as a function of the time interval and fitted to a mono-exponential function. In the presence of the β3-subunit, there was a significantly accelerated time course for recovery (Fig. 8B). The time taken to reach recovery of 50% of the Na^+ channels was reduced to 2.97 ± 0.82 ms with the β3-subunit when compared to 5.29 ± 0.92 ms without the β3-subunit. Consistent with this, the time constant (τ) of recovery was 7.64 ± 1.32 ms for Nav1.5 + EGFP and 4.28 ± 1.19 ms for Nav1.5 + β3-EGFP.

Discussion:

The atomic-resolution structure of the β3-subunit Ig domain indicates that it can trimerize and the isolated Ig domain has been shown to associate in solution with low affinity (3, 10, 19). Super-resolution imaging has also identified full-length β3-subunits assembled as trimers on the plasma membrane of HEK293F cells (10). In view of the striking nature of this interaction, and its potential functional implications, we further explored the self-association of the full-length β3-subunit *in situ* as well as its potential to influence Nav channel assembly and function.

Here we show by co-immunoprecipitation that the oligomeric interaction between β3-subunits expressed in the absence of α-subunit, is sufficiently stable to survive immunoprecipitation. Cross-linking of these samples is consistent with an existence of β3-subunit dimers and trimers rather than aggregated protein (Fig. 1A, B). PLA analysis provides further evidence that full-length β3-subunits, transfected into HEK293F cells can oligomerise. This occurs both at the plasma membrane and within the secretory pathway. Thus, the self-association begins shortly after biosynthesis (Fig. 1C). The trimer interface on the β3-Ig domain contains an extended hydrophobic patch at its N-terminal region, which is held exposed on the protein surface by an intra-subunit disulfide bond (10). Proteins within the ER that contain exposed hydrophobic regions are strong candidates for removal and destruction by the ERAD pathway (20). Early trimer formation within the ER would bury the hydrophobic N-terminal region of β3 and facilitate its export and traffic to the surface. *Cis*-interactions have also been characterised for the Nav channel β4-subunit, independently of its binding to Nav channels. In this case, the cis-interactions between β4-subunits facilitate trans-cell adhesion behaviour (20–22). The β3-subunit has also been shown to promote *trans*-cell adhesion, at least under conditions of high expression (19). Hence, the ability of β3-subunits to homo-trimerize may reflect a more general tendency of Nav channel β-subunits to self-assemble, at least under some *in vivo* conditions – for example, in the absence of Nav α-subunits.

On neuronal cells and cardiomyocytes, Nav channels are known to be restricted into local micro-domain regions of the plasma membrane (24). Furthermore, it has been reported that that these channels may functionally interact under pathological conditions (24, 25). However, in these cases, Nav channel clustering is assumed to reflect heterogeneous and multi-valent molecular interactions between Nav channels themselves and many different cell-specific proteins such as gap-junction proteins, cell-adhesion molecules, cytoskeletal components and other ion channels (26).

Previous evidence suggests that heterologously expressed Nav1.5 α-subunits can assemble as dimers (27–30); and this may be a general behaviour of other Nav channel isoforms (31). The epitope recognised by the antibody used in our STORM experiments is located at the cytoplasmic C-terminus of the Nav1.5 α-subunit. By comparison with other Nav channels whose near atomic-resolution structure has been resolved, it is likely that this epitope lie close to or underneath the central pore of the channel, albeit with some flexibility (32).

Observed from above the membrane, a single α-subunit is an approximate square of length ~ 8 nm (33). Thus, given the uncertainties generated by antibody size and orientation, the single 6 nm modal peak in the nearest-neighbor distribution and the < 10 nm modal peak in the cluster radii distribution for Nav1.5 α-subunits expressed alone (Fig. 2) is consistent with surface-expressed Nav 1.5 α-subunits forming dimers, as the most common arrangement within the clusters. Significantly however, both the cluster radii and nearest-neighbor distributions extended considerably further than these modal values. This indicates an additional layer of supramolecular organisation, within the clusters in which multiple Nav channels lie close together. However, it should be noted, that an accurate estimate of the absolute number of Nav1.5 α-subunits per cluster is not straightforward as nanoscopic stoichiometry is challenging in STORM imaging. The major issues include the unspecific labelling ratio between fluorophore and the protein of interest, and over counting of proteins due to multiple blinks from single fluorophores (34).

We suggest that on the two-dimensional surface of the plasma membrane, the Nav1.5 α-subunit dimers themselves further interact. It is becoming clear that such weak homophilic interactions are common for plasma membrane proteins (35). Such homophilic interactions could explain the fact that several mutations in the Nav1.5 α-subunit that underlie inherited cardiopathologies, act in a strongly dominant-negative capacity, in which the mutant α-subunit binds to and interferes directly with the trafficking and/or gating behaviour of the wild-type channel. Significantly, this occurs even when the mutant and wild-type Nav1.5 channels are co-expressed in HEK293F cells (28, 30). The data presented here indicate that clustering may be an inherent property of Nav1.5 channels.

We have previously suggested that the presence of multiple β3-subunits could act to enhance local Nav1.5 α-subunit oligomerisation on the plasma membrane (3, 10). However, our STORM data indicates that the β3-subunit did not affect the relative proportion of Nav1.5 α-subunits in clusters, nor the relative density of clusters on the plasma membrane (Fig. 2). Nevertheless, the β3-subunit did affect cluster structure. Firstly, it significantly increased the distribution of cluster radii, shifting the modal peak of the distribution from 5-10 nm to a higher peak-radii of 10-15nm. Secondly, it significantly altered the form of the distribution of nearest-neighbor distances between α-subunits within clusters, generating a bimodal distribution with distinct maximum values of ~6 nm and ~12 nm respectively (Fig. 2E). The persistence of the 6 nm peak could suggest that the Nav1.5 α-subunits retain their dimeric association. However, the additional 12 nm modal peak in the nearest-neighbor distribution suggests an additional alteration in the relative arrangement of α-subunits within the clusters, perhaps indicating that β3 is now promoting particular orientations of Nav1.5 α-subunit dimers, within existing clusters.

The presence of β3 generated an enhanced PLA signal between Nav1.5 α-subunits compared to that in the absence of β3 (Fig. 3A, B). Since our STORM data indicated that β3 did not increase the proportion of oligomerised Nav1.5 α-subunits or cluster density (Fig. 2B, C), this suggests that the enhanced PLA signal is

not the result of non-specific 'crowding' caused by over-expression of β3-subunits. By its nature, PLA is a highly sensitive method for detecting protein proximity (18). However, because PLA is based on a DNA amplification protocol, it is inevitably sensitive to even minor differences in factors such as epitope accessibility, not just for the two different labelling antibodies, but also the single-stranded DNA linker and amplification enzymes. Consequently, PLA signals compared under different conditions where the relevant epitopes adopt different relative orientations may not provide rigorously quantitative indications of proximity and should therefore be interpreted with caution (36). For example, there is a strongly enhanced PLA signal recorded for EGF-receptors when they bind EGF ligand. This has been interpreted to indicate that EGF promotes the dimerization of the EGF-receptor (30). However, recent STORM imaging has revealed that even in the absence of EGF, the EGF-receptors form complex oligomers on the plasma membrane, but the EGF binding induced a local geometric rearrangement of these receptors such that the intracellular tyrosine kinase domains could more readily cross-phosphorylate each other (37). Hence, the enhanced PLA signal following EGF binding most likely reflects this local rearrangement in the pre-existing EGF-receptor clusters, rather than ligand-induced receptor dimerization. It should therefore be emphasised that in studying membrane-bound protein assemblies, super-resolution imaging and PLA-type experiments potentially reflect differing aspects of these supramolecular interactions. Furthermore, as detected by standard immunofluorescence, HA-tagged and GFP-tagged Nav1.5 subunits co-localise, both at the plasma membrane and within internal membrane compartments, when they are co-expressed in HEK293F cells (Supplementary Fig. S1). However, the PLA signal is consistently stronger at the plasma membrane (Fig. 3), providing further evidence that the PLA signal intensity reflects not just local Nav channel proximity, but is also sensitive to additional factors such as the relative change in epitope accessibility caused by the influence in the β3-subunit within a specific cellular compartment.

The location of the β3-interaction sites on the Nav channel α-subunit are currently not well-defined. However, we have previously demonstrated that the β3-subunit can potentially bind to the Nav1.5 α-subunit at one or more sites on the transmembrane domain and/or the intracellular region of β3 (13). In the case of Nav1.1, the β3 intracellular region binds to the α-subunit C-terminal domain (38), which lies directly underneath the DIV voltage-sensor (39). The β3 intracellular region is 32 amino acids long and is largely unstructured (5). Therefore, if the β3 intracellular region similarly binds to the Nav1.5 C-terminal domain, then one of the β3-binding sites on the α-subunit must lie within a radius of no more than about 7 - 8 nm from the α subunit C-terminal domain. The voltage sensors from DI, DIII and DIV all lie comfortably within this distance (39).

Further insights have also recently been provided from cryo-EM structures of the eel and human Nav1.4 channel α-subunits and their associations with a single β1-subunit (33, 40). Here, the transmembrane domain of the β1-subunit interacts with the S1 and S2 transmembrane helices of the DIII voltage sensor and the Ig domain forms salt-bridges with a short extracellular loop between these two helices. This α-subunit binding

site on the β1 Ig domain includes a region of the N-terminus that shows sequence conservation with the trimer interface of β3. Therefore, if a β3-subunit Ig domain were to bind to the α-subunit at this location - and in the same manner as β1 - then it would not be able to form a trimer with other β3-subunits. However, AFM images indicate that under conditions of high expression, the β3-subunit can bind at up to four separate sites symmetrically arranged around the Nav1.5 α-subunit (10), a finding that is consistent with recent electrophysiological work that indicated more than one binding site for β3 on the Nav1.5 α-subunit (41). The presence of multiple β-subunits around the α-subunit is likely to increase the effective 'footprint' of a Nav1.5 complex and could provide a simple explanation for the increased radii distribution shown in Fig. 2D.

We found that β3-subunits had no significant effect on the $V_{½}$ of steady-state activation (Fig. 4 and Table 1) but showed clear and significant depolarising effects on the $V_{½}$ of steady-state inactivation (Fig. 5 and Table 1). In contrast, the slope factors (*k*) of both steady-state activation and inactivation remain unchanged. The slope factor term is classically attributed to the effective charge transfer (*z*) involved in transitions between resting and activated, and activated and inactivated Nav channels through the equation: $k = RT / zF$ (R is the Gas constant; T is the absolute temperature and F is the Faraday constant) (42). The values of *k* for both activation and inactivation corresponded to charge transfers of *z* between 3 and 4 and were accordingly in agreement with values obtained from other studies and in other systems (2, 43). These findings are consistent with such charged groups on individual α-subunits, likely those underlying respective voltage sensors, remaining sufficiently functionally far apart within the clusters, so as not to be altered by the presence of β3.

A similarly selective electrophysiological effect of β3 on Nav1.5 inactivation has been reported when studied in *Xenopus* oocytes (4, 41). It is also consistent with data from the $Scn3b^{-/-}$ mouse model that lacks β3 expression and shows distinctive conduction abnormalities (7, 8). Thus, the electrophysiological effects described here mimic key features of the channel behaviour in a whole animal model. The DIV voltage sensor is known to play a major role in the modulation of the voltage-dependence of inactivation (1). Our data suggests that at least one of the electrophysiologically important β3-binding sites will lie close to this region. As noted above, a β3 molecule tethered to the α-subunit by its intracellular region will lie close to the DIV voltage sensor where it could affect voltage-dependence of inactivation.

Such functional independence between clustered Nav1.5 α-subunits extend to the kinetic properties of Hodgkin-Huxley modelling, in which β3 co-expression failed to exert significant effects on the time constants for activation and inactivation. This suggests that the geometric rearrangement of the Nav1.5 channels driven by the β3-subunit did not change any functional coupling between α-subunits (Fig. 6 and Fig. 7). The β3-subunit did significantly accelerate recovery from inactivation (Fig. 8). However, the α-subunit C-terminal domain binds to both the α-subunit inactivation gate (44) and to the intracellular region of β3 (38). Hence, the recovery from inactivation data could be more simply explained by interactions between a single α- and a single associated β3-subunit, rather than cooperative interactions between different α-subunits.

If Nav1.5 channels clustered together independently of β3, then any role for β3 must reflect other features of Nav channel biology. For example, the depolarising shift in $V_{1/2}$ inactivation caused by β3 implies that the electric field detected by the inactivation sensor has increased, the physiological consequence of which will be to increase the number of channels that remain activatable at a given voltage. If under these circumstances, the Nav1.5 α-subunits are locally clustered, it will increase the local density of channels on a given patch of membrane and therefore increase the maximum density of sodium current capable of being delivered through that local patch. It is also possible that organising Nav channels into clustered units will reduce the rate of channel endocytosis, and further enhance local channel density.

In conclusion, our data indicates that under conditions typical of many published electrophysiological studies, Nav1.5 channels exist as multimers both in the presence and absence of the β3-subunit. It will be interesting to see if this phenomenon holds for other cell systems. For example, in cellular expression systems such as CHO and COS cells, β3 produces hyperpolarising shifts in $V_{1/2}$ of both activation and inactivation for Nav1.5 (6, 9, 13). The reasons for this opposite and strikingly different behavior compared to HEK293F cells, oocytes and native cardiomyocytes are completely unknown, but it could involve differences in post-translational modifications and/or accessory proteins. But it could also involve different degrees of heterogenetity in Nav channel oligomerization. At a time when near atomic-resolution structures for Nav channels are beginning to be solved, we emphasize that the supramolecular organisation of the channels on the cellular plasma membrane should also be considered.

Author contributions:

SCS, AJT, CLHH and APJ designed research; SCS, AMcS and JRI performed the experimental work; MH, LW, CT and MM-F analysed and interpreted the super-resolution imaging data, MWR and RB developed software for data analysis and SCS, JSR, AJT, CLHH and APJ interpreted the data. SCS, CLHH and APJ wrote the paper.

Acknowledgements:

We would like to thank the Gurdon Institute Imaging Facility for use of their microscope and general assistance. This work was supported by a British Heart Foundation grant (PG/14/79/31102) to APJ and CLHH, The Wellcome Trust, award number: 105727/Z/14/Z to CLHH and a Medical Research Council grant (MR/K015591/1) to CLF, RAL, STFC. The authors declare no competing interests.

References

1. Ahern, C. A., Payandeh, J., Bosmans, F., and Chanda, B. (2016) The hitchhiker's guide to the voltage-gated sodium channel galaxy. *J. Gen. Physiol.* **147**, 1–24

2. Hodgkin, A. L., and Huxley, A. F. (1952) A quantitative description of membrane current and its application to conduction and excitation in nerve. *J. Physiol.* **117**, 500–44

3. Namadurai, S., Yereddi, N. R., Cusdin, F. S., Huang, C. L.-H., Chirgadze, D. Y., and Jackson, A. P. (2015) A new look at sodium channel β subunits. *Open Biol.* **5**, 140192

4. Fahmi, A. I., Patel, M., Stevens, E. B., Fowden, A. L., John, J. E., Lee, K., Pinnock, R., Morgan, K., Jackson, A. P., and Vandenberg, J. I. (2001) The sodium channel beta-subunit SCN3b modulates the kinetics of SCN5a and is expressed heterogeneously in sheep heart. *J. Physiol.* **537**, 693–700

5. Cusdin, F. S., Nietlispach, D., Maman, J., Dale, T. J., Powell, A. J., Clare, J. J., and Jackson, A. P. (2010) The Sodium Channel 3-Subunit Induces Multiphasic Gating in NaV1.3 and Affects Fast Inactivation via Distinct Intracellular Regions. *J. Biol. Chem.* **285**, 33404–33412

6. Ko, S. H., Lenkowski, P. W., Lee, H. C., Mounsey, J. P., and Patel, M. K. (2005) Modulation of Nav1.5 by β1- and β3-subunit co-expression in mammalian cells. *Pflugers Arch. Eur. J. Physiol.* **449**, 403–412

7. Hakim, P., Brice, N., Thresher, R., Lawrence, J., Zhang, Y., Jackson, A. P., Grace, A. A., and Huang, C. L.-H. (2010) Scn3b knockout mice exhibit abnormal sino-atrial and cardiac conduction properties. *Acta Physiol. (Oxf).* **198**, 47–59

8. Hakim, P., Gurung, I. S., Pedersen, T. H., Thresher, R., Brice, N., Lawrence, J., Grace, A. A., and Huang, C. L.-H. (2008) Scn3b knockout mice exhibit abnormal ventricular electrophysiological properties. *Prog. Biophys. Mol. Biol.* **98**, 251–266

9. Ishikawa, T., Takahashi, N., Ohno, S., Sakurada, H., Nakamura, K., On, Y. K., Park, J. E., Makiyama, T., Horie, M., Arimura, T., Makita, N., and Kimura, A. (2013) Novel SCN3B mutation associated with brugada syndrome affects intracellular trafficking and function of Nav1.5. *Circ. J.* **77**, 959–67

10. Namadurai, S., Balasuriya, D., Rajappa, R., Wiemhöfer, M., Stott, K., Klingauf, J., Edwardson, J. M., Chirgadze, D. Y., and Jackson, A. P. (2014) Crystal structure and molecular imaging of the Nav channel β3 subunit indicates a trimeric assembly. *J. Biol. Chem.* **289**, 10797–811

11. Balasuriya, D., Stewart, A. P., Crottès, D., Borgese, F., Soriani, O., and Edwardson, J. M. (2012) The sigma-1 receptor binds to the Nav1.5 voltage-gated Na+ channel with 4-fold symmetry. *J. Biol. Chem.* **287**, 37021–9

12. Cusdin, F. S., Nietlispach, D., Maman, J., Dale, T. J., Powell, A. J., Clare, J. J., and Jackson, A. P. (2010) The sodium channel {beta}3-subunit induces multiphasic gating in NaV1.3 and affects fast inactivation via distinct intracellular regions. *J. Biol. Chem.* **285**, 33404–12

13. Yu, E. J., Ko, S.-H., Lenkowski, P. W., Pance, A., Patel, M. K., and Jackson, A. P. (2005) Distinct domains of the sodium channel beta3-subunit modulate channel-gating kinetics and subcellular location. *Biochem. J.* **392**, 519–26

14. Roberts, S., Hirsch, M., McStea, A., Zanetti-Domingues, L., Clarke, D., Claus, J., Parker, P., Wang, L., and Martin-Fernandez, M. (2018) Cluster Analysis of Endogenous HER2 and HER3 Receptors in SKBR3 Cells. *BIO-PROTOCOL*. 10.21769/BioProtoc.3096

15. Corder, G. W., and Foreman, D. I. *Nonparametric statistics : a step-by-step approach*

16. Schindelin, J., Arganda-Carreras, I., Frise, E., Kaynig, V., Longair, M., Pietzsch, T., Preibisch, S., Rueden, C., Saalfeld, S., Schmid, B., Tinevez, J.-Y., White, D. J., Hartenstein, V., Eliceiri, K., Tomancak, P., and Cardona, A. (2012) Fiji: an open-source platform for biological-image analysis. *Nat. Methods*. **9**, 676–682

17. Allalou, A., and Wählby, C. (2009) BlobFinder, a tool for fluorescence microscopy image cytometry. *Comput. Methods Programs Biomed.* **94**, 58–65

18. Söderberg, O., Gullberg, M., Jarvius, M., Ridderstråle, K., Leuchowius, K.-J., Jarvius, J., Wester, K., Hydbring, P., Bahram, F., Larsson, L.-G., and Landegren, U. (2006) Direct observation of individual endogenous protein complexes in situ by proximity ligation. *Nat. Methods*. **3**, 995–1000

19. Yereddi, N. R., Cusdin, F. S., Namadurai, S., Packman, L. C., Monie, T. P., Slavny, P., Clare, J. J., Powell, A. J., and Jackson, A. P. (2013) The immunoglobulin domain of the sodium channel β3 subunit contains a surface-localized disulfide bond that is required for homophilic binding. *FASEB J.* **27**, 568–80

20. Printsev, I., Curiel, D., and Carraway, K. L. (2017) Membrane Protein Quantity Control at the Endoplasmic Reticulum. *J. Membr. Biol.* **250**, 379–392

21. Malhotra, J. D., Kazen-Gillespie, K., Hortsch, M., and Isom, L. L. (2000) Sodium channel beta subunits mediate homophilic cell adhesion and recruit ankyrin to points of cell-cell contact. *J. Biol. Chem.* **275**, 11383–8

22. Shimizu, H., Miyazaki, H., Ohsawa, N., Shoji, S., Ishizuka-Katsura, Y., Tosaki, A., Oyama, F., Terada, T., Sakamoto, K., Shirouzu, M., Sekine, S., Nukina, N., and Yokoyama, S. (2016) Structure-based site-directed photo-crosslinking analyses of multimeric cell-adhesive interactions of voltage-gated sodium channel β subunits. *Sci. Rep.* **6**, 26618

23. Shimizu, H., Tosaki, A., Ohsawa, N., Ishizuka-Katsura, Y., Shoji, S., Miyazaki, H., Oyama, F., Terada, T., Shirouzu, M., Sekine, S., Nukina, N., and Yokoyama, S. (2017) Parallel homodimer structures of the extracellular domains of the voltage-gated sodium channel β4 subunit explain its role in cell–cell adhesion. *J. Biol. Chem.* **292**, 13428–13440

24. Catterall, W. a, and Morrow, C. S. (1978) Binding to saxitoxin to electrically excitable neuroblastoma cells. *Proc. Natl. Acad. Sci. U. S. A.* 10.1073/pnas.75.1.218

25. Undrovinas, A. I., Fleidervish, I. A., and Makielski, J. C. (1992) Inward sodium current at resting potentials in single cardiac myocytes induced by the ischemic metabolite lysophosphatidylcholine. *Circ. Res.* **71**, 1231–1241

26. Balse, E., and Eichel, C. (2017) The Cardiac Sodium Channel and Its Protein Partners. in *Handbook of experimental pharmacology*, pp. 73–99, **246**, 73–99

27. Clatot, J., Ziyadeh-Isleem, A., Maugenre, S., Denjoy, I., Liu, H., Dilanian, G., Hatem, S. N., Deschênes, I., Coulombe, A., Guicheney, P., and Neyroud, N. (2012) Dominant-negative effect of SCN5A N-terminal mutations through the interaction of Na(v)1.5 α-subunits. *Cardiovasc. Res.* **96**, 53–63

28. Clatot, J., Zheng, Y., Girardeau, A., Liu, H., Laurita, K. R., Marionneau, C., and

Deschênes, I. (2018) Mutant voltage-gated Na + channels can exert a dominant negative effect through coupled gating. *Am. J. Physiol. Circ. Physiol.* **315**, H1250–H1257

29. Clatot, J., Hoshi, M., Wan, X., Liu, H., Jain, A., Shinlapawittayatorn, K., Marionneau, C., Ficker, E., Ha, T., and Deschênes, I. (2017) Voltage-gated sodium channels assemble and gate as dimers. *Nat. Commun.* **8**, 2077

30. Poelzing, S., Forleo, C., Samodell, M., Dudash, L., Sorrentino, S., Anaclerio, M., Troccoli, R., Iacoviello, M., Romito, R., Guida, P., Chahine, M., Pitzalis, M., and Deschênes, I. (2006) SCN5A polymorphism restores trafficking of a Brugada syndrome mutation on a separate gene. *Circulation*. 10.1161/CIRCULATIONAHA.105.601294

31. Rühlmann, A. H., Körner, J., Bebrivenski, N., Detro-Dassen, S., Hautvast, P., Benasolo, C. A., Meents, J., Machtens, J.-P., Schmalzing, G., and Lampert, A. (2019) Uncoupling sodium channel dimers rescues phenotype of pain-linked Nav1.7 mutation. *bioRxiv*. 10.1101/716654

32. Shen, H., Li, Z., Jiang, Y., Pan, X., Wu, J., Cristofori-Armstrong, B., Smith, J. J., Chin, Y. K. Y., Lei, J., Zhou, Q., King, G. F., and Yan, N. (2018) Structural basis for the modulation of voltage-gated sodium channels by animal toxins. *Science (80-.).* 10.1126/science.aau2596

33. Pan, X., Li, Z., Zhou, Q., Shen, H., Wu, K., Huang, X., Chen, J., Zhang, J., Zhu, X., Lei, J., Xiong, W., Gong, H., Xiao, B., and Yan, N. (2018) Structure of the human voltage-gated sodium channel Nav1.4 in complex with β1. *Science (80-.).* **362**, eaau2486

34. Durisic, N., Cuervo, L. L., and Lakadamyali, M. (2014) Quantitative super-resolution microscopy: Pitfalls and strategies for image analysis. *Curr. Opin. Chem. Biol.* 10.1016/j.cbpa.2014.04.005

35. Saka, S. K., Honigmann, A., Eggeling, C., Hell, S. W., Lang, T., and Rizzoli, S. O. (2014) Multi-protein assemblies underlie the mesoscale organization of the plasma membrane. *Nat. Commun.* **5**, 4509

36. Aslemarz, A., Lasko, P., and Fagotto, F. (2018) Limited significance of the in situ proximity ligation assay. *bioRxiv*. 10.1101/411355

37. Zanetti-Domingues, L. C., Korovesis, D., Needham, S. R., Tynan, C. J., Sagawa, S., Roberts, S. K., Kuzmanic, A., Ortiz-Zapater, E., Jain, P., Roovers, R. C., Lajevardipour, A., van Bergen en Henegouwen, P. M. P., Santis, G., Clayton, A. H. A., Clarke, D. T., Gervasio, F. L., Shan, Y., Shaw, D. E., Rolfe, D. J., Parker, P. J., and Martin-Fernandez, M. L. (2018) The architecture of EGFR's basal complexes reveals autoinhibition mechanisms in dimers and oligomers. *Nat. Commun.* **9**, 4325

38. Spampanato, J., Kearney, J. A., de Haan, G., McEwen, D. P., Escayg, A., Aradi, I., MacDonald, B. T., Levin, S. I., Soltesz, I., Benna, P., Montalenti, E., Isom, L. L., Goldin, A. L., and Meisler, M. H. (2004) A Novel Epilepsy Mutation in the Sodium Channel SCN1A Identifies a Cytoplasmic Domain for Subunit Interaction. *J. Neurosci.* **24**, 10022–10034

39. Shen, H., Zhou, Q., Pan, X., Li, Z., Wu, J., and Yan, N. (2017) Structure of a eukaryotic voltage-gated sodium channel at near-atomic resolution. *Science (80-.).* **355**, eaal4326

40. Yan, Z., Zhou, Q., Wang, L., Wu, J., Zhao, Y., Huang, G., Peng, W., Shen, H., Lei, J., and Yan, N. (2017) Structure of the Na v 1.4-β1 Complex from Electric Eel. *Cell*. **170**, 470-482.e11

41. Zhu, W., Voelker, T. L., Varga, Z., Schubert, A. R., Nerbonne, J. M., and Silva, J. R. (2017) Mechanisms of noncovalent β subunit regulation of Na V channel gating. *J. Gen. Physiol.* **149**, 813–831

42. Adrian, R. H. (1978) Charge Movement in the Membrane of Striated Muscle. *Annu. Rev. Biophys. Bioeng.* **7**, 85–112

43. Adrian, R. H., Chandler, W. K., and Hodgkin, A. L. (1969) The kinetics of mechanical activation in frog muscle. *J. Physiol.* **204**, 207–30

44. Motoike, H. K., Liu, H., Glaaser, I. W., Yang, A.-S., Tateyama, M., and Kass, R. S. (2004) The Na + Channel Inactivation Gate Is a Molecular Complex. *J. Gen. Physiol.* **123**, 155–165

	Activation			Inactivation			Recovery from Inactivation		
	$V_{½}$ (mV)	*k* (mV)	n	$V_{½}$ (mV)	*k* (mV)	n	τ (ms)	$t_{½}$ (ms)	n
Nav1.5 + EGFP	-42.62 ± 1.81	7.28 ± 0.61	8	-96.14 ± 0.72	-7.17 ± 0.20	27	7.64 ± 1.32	5.29 ± 0.92	7
Nav1.5 + β3-EGFP	-42.61 ± 1.67	9.42 ± 0.94	10	-90.64 ± 1.02***	6.47 ± 0.32	20	4.28 ± 1.19***	2.97 ± 0.82***	10

Table 1. Nav1.5 channel gating alone or with β3 co-expressed. Parameters are derived from the Boltzmann function fit to steady-state activation and inactivation data, and from a mono-exponential function for recovery from inactivation data. Data are means ± SEM, statistically significant results were determined using unpaired t-tests; *** $P > 0.001$ vs. Nav1.5 + EGFP

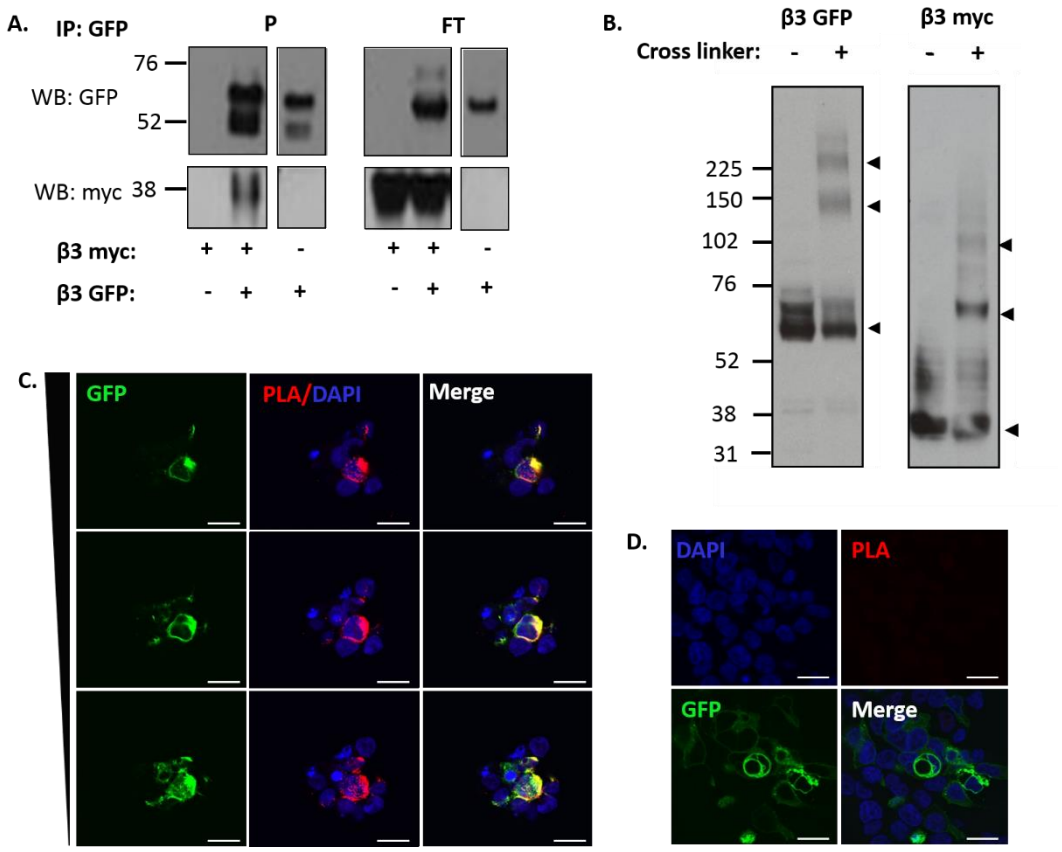

Figure 1. Oligomerisation of β3. A. Co-IP of overexpressed β3-EGFP and β3-myc from singly or co-transfected HEK293F cell lysates. β3-myc only appeared in the bound fraction when co-expressed with β3-EGFP. P = 'pellet', ie bound fraction; FT = 'flow through' ie non-bound fraction. **B.** Cross-linking of singly expressed β3-EGFP and β3-myc subunits. In the absence of the crosslinking agent (BS3) only bands consistent with the monomer (lower arrow-head), ~56-60 kDa and ~36-38 kDa for β3-EGFP and β3-myc respectively, and glycosylation states were observed. Chemical cross-linking resulted in multiple bands, consistent with the monomeric, dimeric (~ 120 kDa and ~ 72 kDa, middle arrowhead) and trimeric (~ 180 kDa and ~110 kDa, upper arrowhead) forms, and glycosylation states. **C.** Proximity ligation assay (PLA) of β3-myc and β3-EGFP. Oligomerisation of β3 *in* situ is demonstrated by the amplification of PLA signals, seen throughout the cell and plasma membrane through a series of z-stacks (left hand panel: top to bottom at 1.8 µm intervals), when β3-myc is co-expressed with β3-EGFP. D. Expression of β3-EGFP alone (right hand panels) did not produce the characteristic punctate red signal typical of PLA tagged proteins within 40 nm of each other. Scale bar = 20 µm. Distance through the z stack is indicated by the tapering bar on the left-hand side of panel **C.**

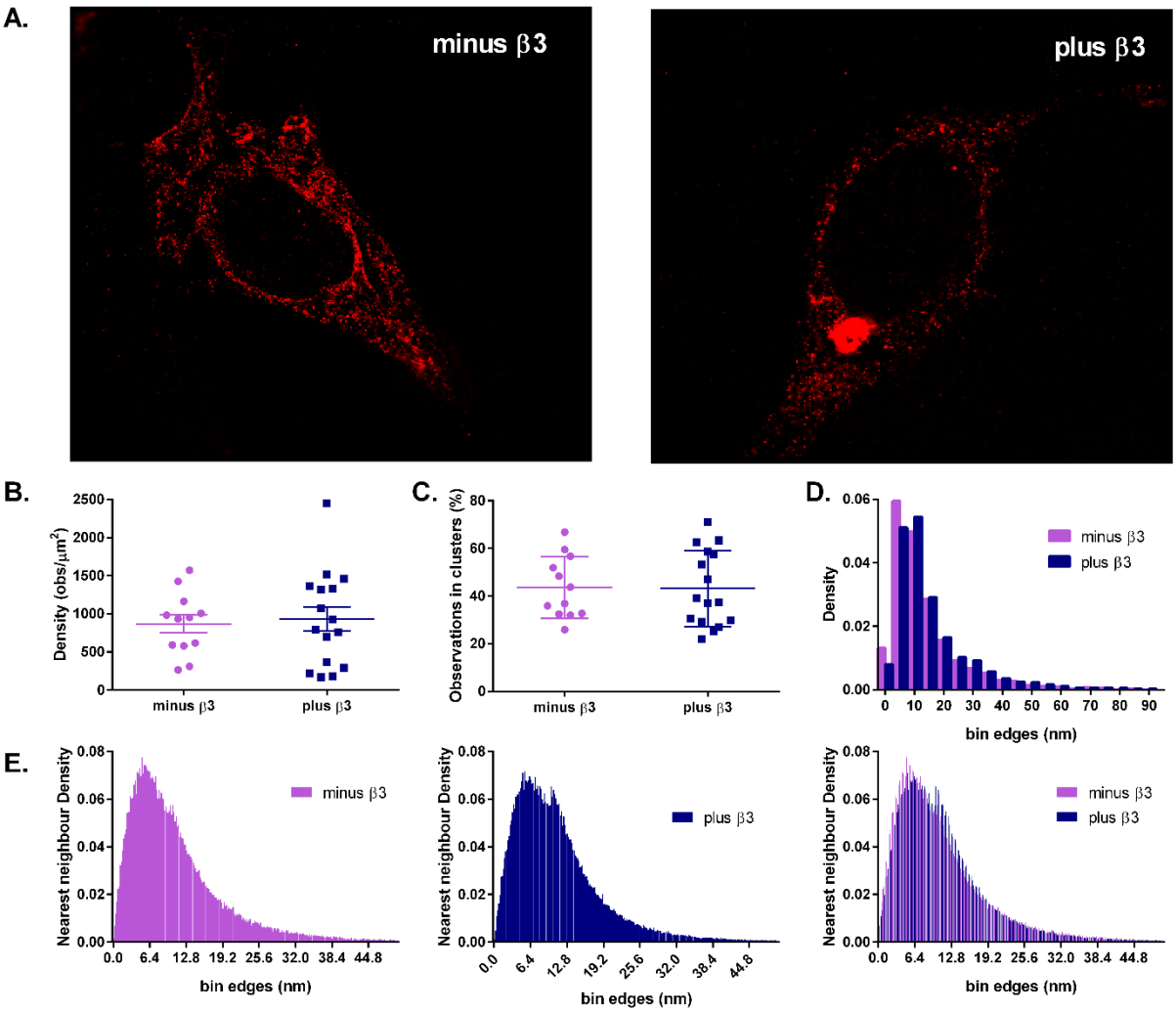

Figure 2. Super-resolution STORM imaging and cluster and nearest neighbour analysis of Nav1.5 α-subunits with and without β3-subunit A. Representative reconstructed images of fluorophore AF-647 blinking in HEK293FF cells co-transfected with Nav1.5-HA/EGFP and Nav1.5-HA/β3-EGFP. B. The percentage of total blinking events that were observed in the same area (cluster) as other blinking events (i.e reflecting colocalised Nav1.5 channels) in the presence and absence of β3. C. The density of blinking events observed per unit area (μm²) for cells expressing Nav1.5-HA, plus and minus β3. D. Normalised cluster radii distribution density for cells expressing Nav1.5-HA plus and minus β3. E. Normalised nearest neighbor distance density between Nav1.5-HA molecules for cells expressing Nav1.5-HA, plus and minus β3, both individually and superimposed. In D., differences between the histogram distributions with and without β3 were tested using the two-sample Kolmogorov-Smirnov test, giving a P value of 4×10^{-9}. In E., differences between the histogram distributions with and without β3 were tested using the two-sample Kolmogorov-Smirnov test, giving a P value of ~ 0.

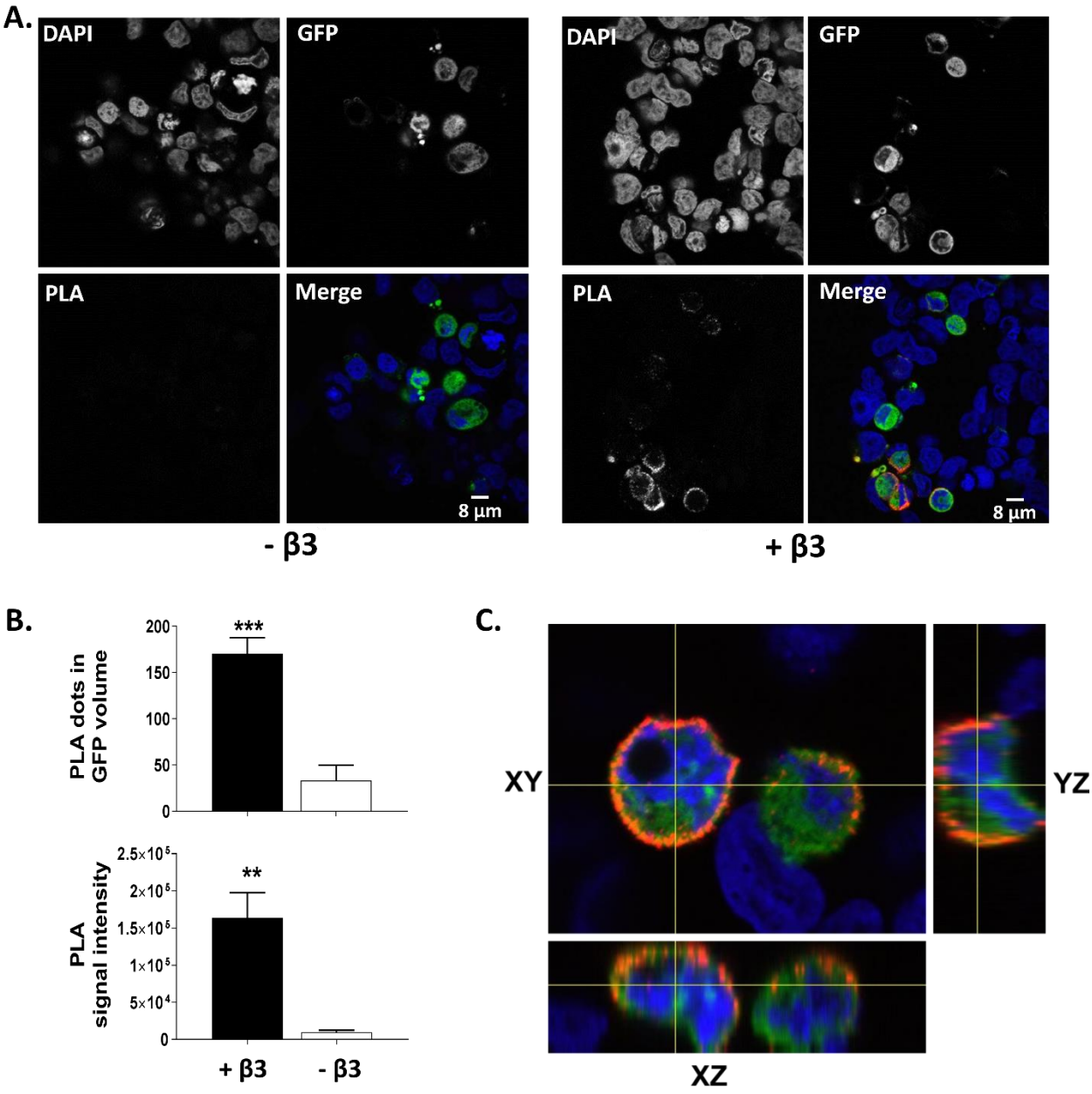

Figure 3. Enhanced oligomerisation of Nav1.5 alpha by β3. A. Representative PLA images of Nav1.5 EGFP and Nav1.5 HA in the absence (left hand panels) and presence (right hand panels) of β3-myc. Although not visible to the naked eye, a number of PLA signals can be detected by ImageJ and blobfinder in the absence of β3 and is recorded in the histograms. B. Quantification of PLA 'dots' within the EGFP volume and PLA signal intensity (mean ± SEM). C. Orthogonal views from sequential images of the PLA signal (red) through the z-stack in cells expressing Nav1.5 EGFP, Nav1.5 H.A and β3-myc, highlighting a predominant, but not exclusive, localisation of PLA signal at the plasma membrane. To compare the expression levels of Nav1.5 EGFP and Nav1.5 H.A in these cells, see Supplementary Fig. S1.

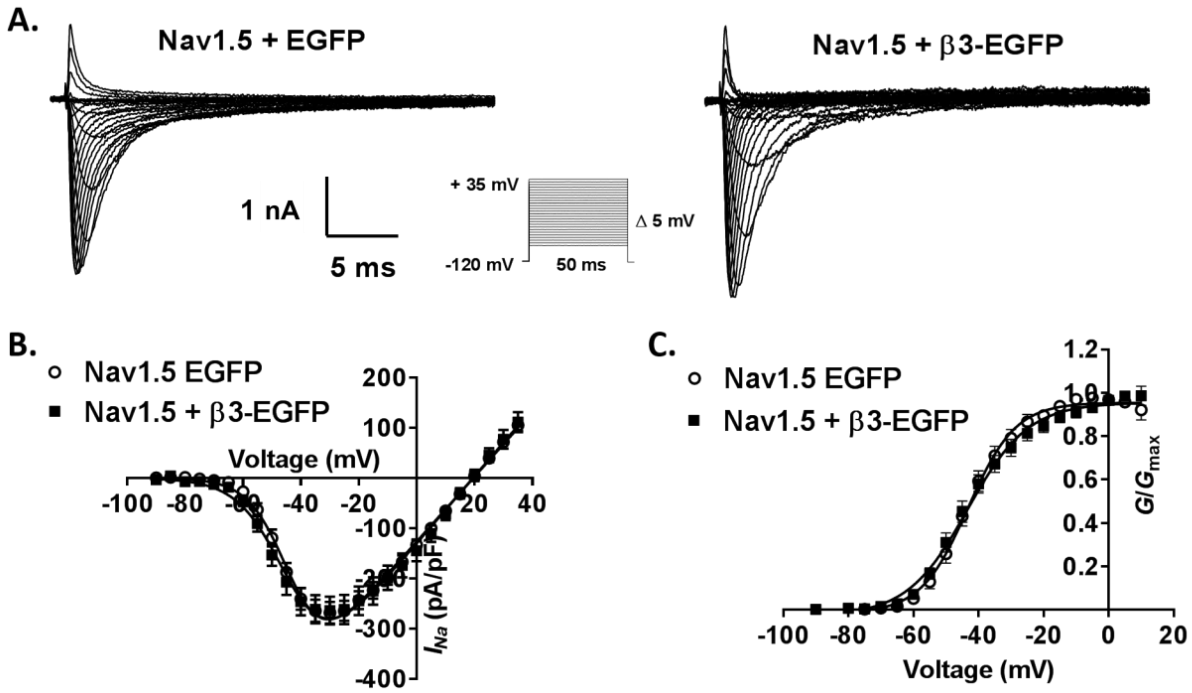

Figure 4. Steady-state activation in Nav1.5 HEK293F cells with and without β3 co-expression. A. Representative whole cell Na^+ currents of Nav1.5-HEK293F cells transfected with EGFP or β3-EGFP in response to depolarising steps (50 ms duration) from a holding potential of -120 mV to test pulses between -90 mV to + 35 mV in 5 mV increments. Cell capacitances of these patches were 10.4 pF and 13.1 pF for Nav1.5 + EGFP and Nav1.5 + B3EGFP respectively. B. *I*/V curves with currents normalised to cell capacitance for EGFP (open circles) and β3-EGFP (closed squares) show no effect of β3. C. Channel conductance as a function of voltage fit with a Boltzmann function (Equation 2), showing no shift in $V_{½}$ or *k* with β3. Means ± SEM, n = 8 and 10 for Nav1.5-EGFP and Nav1.5-B3 EGFP respectively.

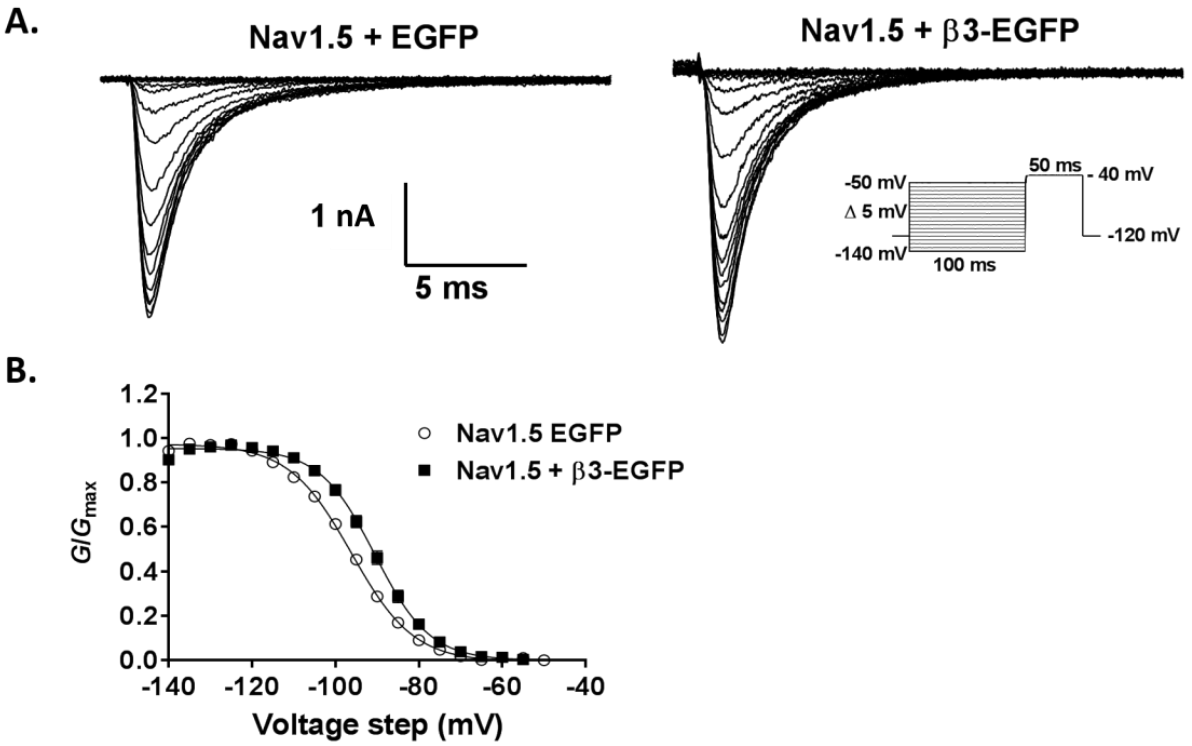

Figure 5. Steady-state inactivation in Nav1.5 HEK293F cells with and without β3 co-expression. A. Representative whole cell Na^+ currents of Nav1.5-HEK293F cells transfected with EGFP or β3-EGFP in response to a test pulse of -40 mV (50 ms duration) immediately subsequent to a pre-pulse step (100 ms duration) to voltages ranging from -140 mV to -50 mV in 5 mV increments. Cell capacitances of these patches were 10.4 pF and 13.1 pF for Nav1.5 + EGFP and Nav1.5 + B3EGFP respectively. B. Inactivation curves reflecting channel availability (G/G_{max}) as a function of the pre-pulse voltage step, means ± SEM, n=27 and 20 for Nav1.5-EGFP and Nav1.5-B3 EGFP respectively. Solid lines are the fits to a Boltzmann function (Equation 2) highlighting a depolarising shift in the voltage-dependence of inactivation with the presence of β3.

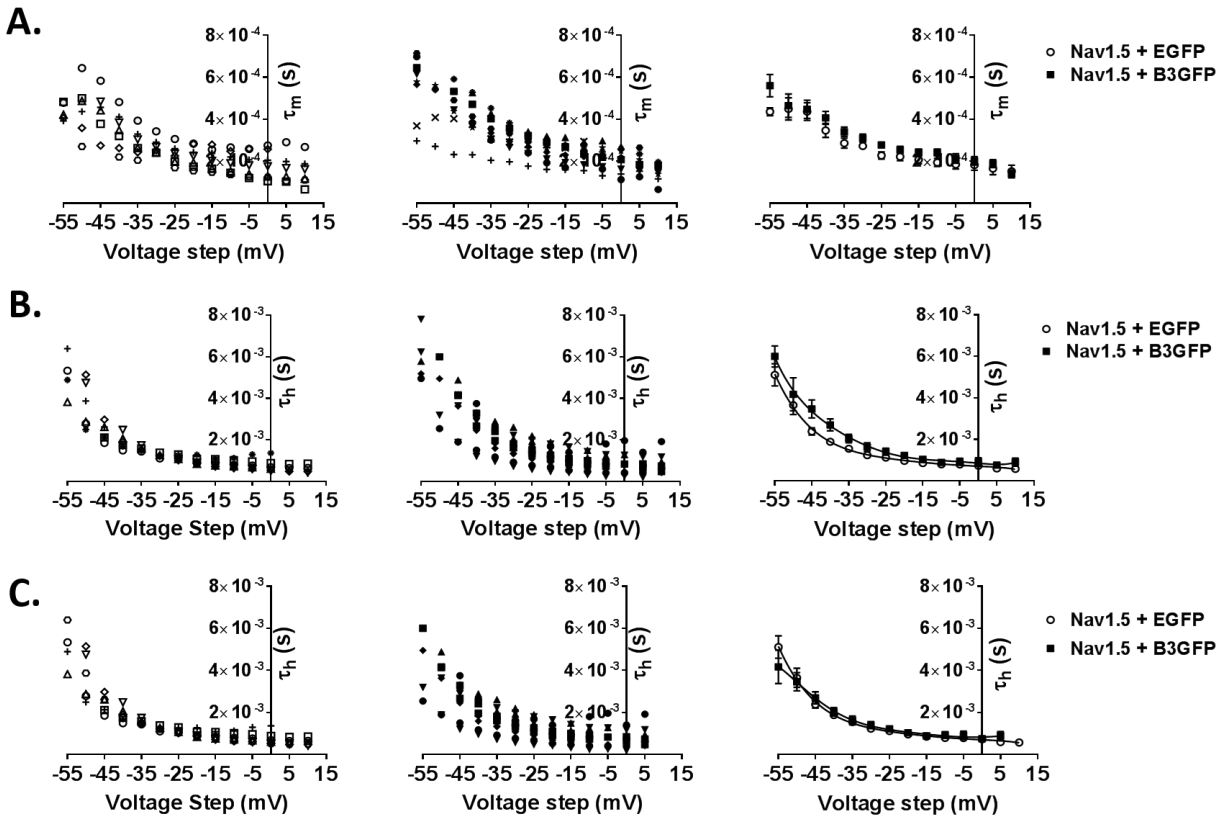

Figure 6. Hodgkin-Huxley kinetics; time constants of the activation and inactivation gates with and without β3 co-expression. A. The time constants of activation (τ_m) with and without β3. B. The time constant of inactivation (τ_h) with and without β3. C. τ_h of the β3 containing Nav1.5-HEK293F cells corrected for the observed shift (5.5mV) in steady-state inactivation.

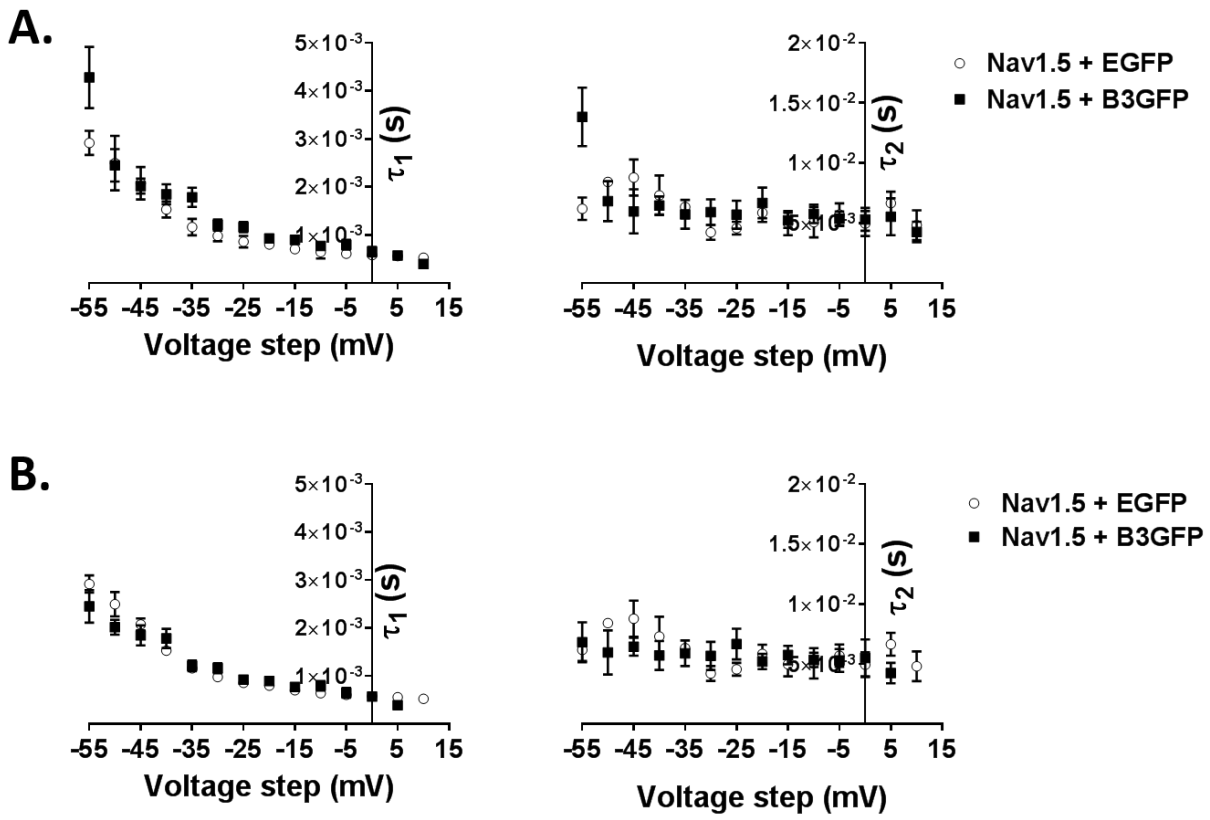

Figure 7. Time constants of inactivation with and without β3 co-expression. Current decays from the steady-state activation protocol were fitted with a double exponential to give both the fast (τ_1) and slow (τ_2) time constants of inactivation in the presence and absence of the β3-subunit. A. τ_1 plotted as a function of the test voltage demonstrates a voltage-dependence irrespective of whether the β3-subunit is present (left panel). In contrast τ_2 is relatively voltage-insensitive of β3 presence. B. The time constants for β3 are shifted by -5 mv to account for the depolarising shift observed in steady-state inactivation.

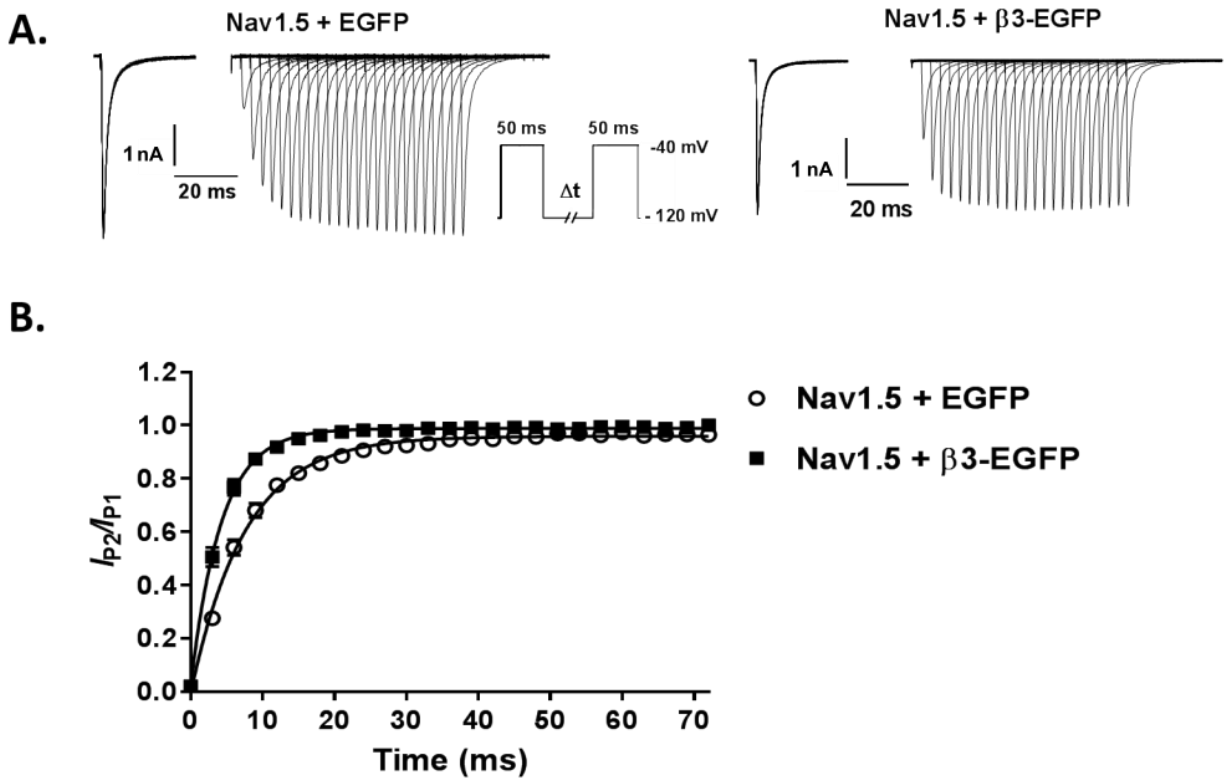

Figure 8. Recovery from inactivation with and without β3 co-expression. A. Typical whole cell Na^+ currents of Nav1.5-HEK293F cells transfected with EGFP or β3-EGFP in response to voltage pulse (-40 mV, 50 ms) at varying time intervals (0-72 ms, in 3 ms increments). B. Peak currents of the test pulse normalised to the conditioning pulse (I_{P2} / I_{P1}) plotted as a function of recovery time. Solid lines are mono-exponential fits highlighting an accelerated recovery time in the β3-EGFP containing cells. *n* = 7, Nav1.5 + EGFP; *n* = 10, Nav1.5 + β3-EGFP

Double labelling IHC

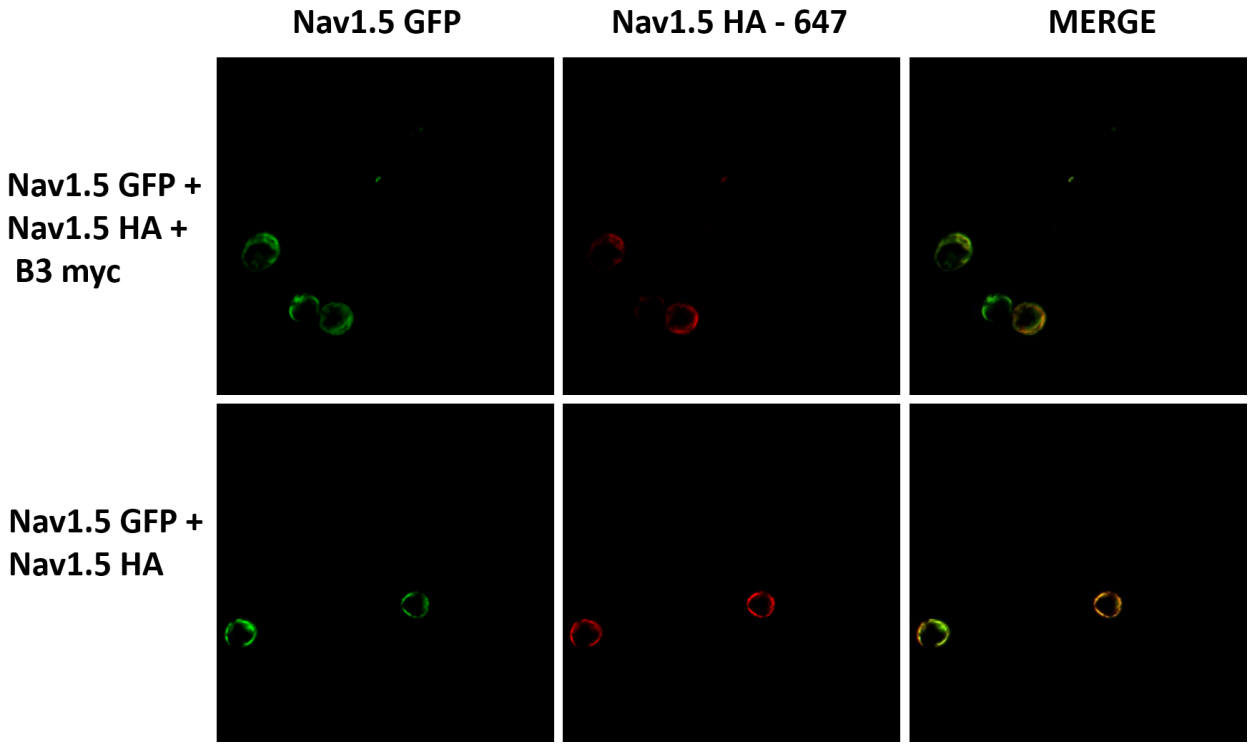

Supplementary Figure S1. Co-expression of Nav1.5-GFP and Nav1.5-H.A. in the presence and absence of β3-Myc. Immunohistochemistry was performed on Nav1.5-H.A. with a fluorescent (Alexa Flour 647) secondary anti